Research Article

In silico studies on structural, functional, and evolutionary analysis of bacterial chromate reductase family responsible for high chromate bioremediation efficiency

Manish Paul[1] · **Payel Puthal Pranjaya**[1] · **Hrudayanath Thatoi**[1]

Received: 13 August 2020 / Accepted: 3 November 2020 / Published online: 13 November 2020

Abstract
In the present study, sequence and structural aspects of five bacterial chromate reductase-related enzymes from *Escherichia coli, Pseudomonas putida, Shigella flexneri,* and *Synechocystis* sp. have been investigated. Comparative sequence analyses of different chromate reductase family enzymes showed that Ser13 in *E. coli* quinone reductase remains conserved among most of the homologous proteins and plays an important role in Flavin mononucleotide (FMN) binding. Comparative protein–ligand binding energy calculation from the docking of all the five modeled complexes of bacterial chromate reductase-related enzymes depicted that quinone reductase from *S. flexneri* has the highest binding affinity (−7.97 kcal/mol) with FMN. Molecular interactions study suggested that the quinone reductase from *P. putida* has the highest number of bonded interactions with FMN. In silico mutation design (Y85N) in *E. coli* ChrR confirmed the significant role of Tyr85 residue in maintaining the network established at the tetramer interface of this enzyme during substrate interaction. Analyses from molecular simulation trajectories also suggested that the mutant *E. coli* ChrR is much stable than the wild-type form during the interaction with substrate FMN. The present study revealed the interrelationship between the structure and function of bacterial chromate reductase-related enzymes which will help to understand their importance in chromium bioremediation.

Manish Paul and Payel Puthal Pranjaya have contributed equally to this work.

Electronic supplementary material The online version of this article (https://doi.org/10.1007/s42452-020-03830-8) contains supplementary material, which is available to authorised users.

✉ Hrudayanath Thatoi, hnthatoi@gmail.com | [1]Department of Biotechnology, North Orissa University, Baripada, Odisha 757003, India.

Graphic abstract

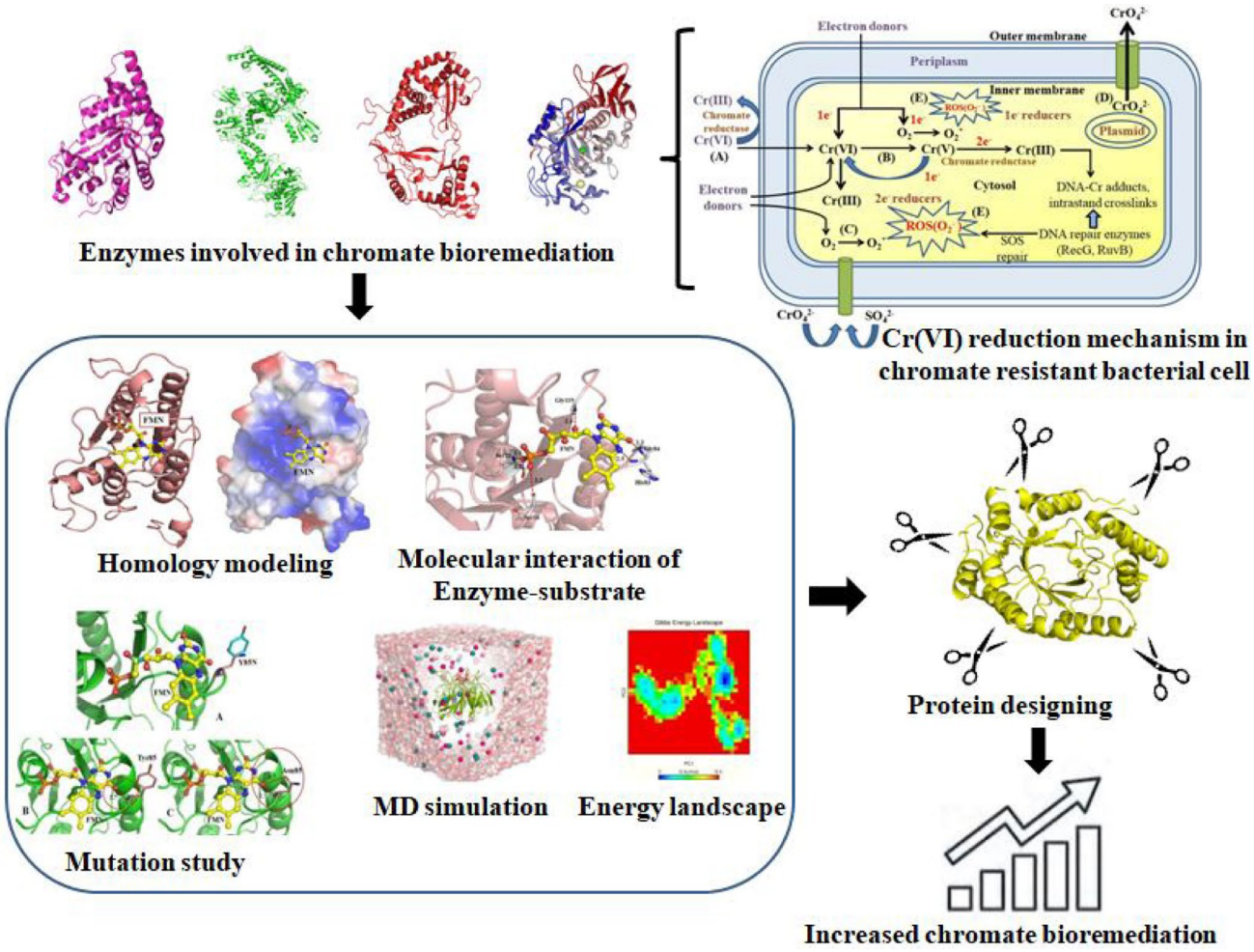

Keywords Bioremediation · Molecular docking · Molecular modeling · Protein dynamism · Quinone reductase

1 Introduction

Global industrialization and urbanization along with several natural processes have led to a serious threat to the ecosystem due to the contamination of toxic heavy metal ions. Heavy metals being a major category of globally-distributed pollutants, as well as detrimental to both humans and other living organisms. Chromium, a naturally occurring heavy metal commonly used in many industrial manufacturing processes is responsible for major industrial and environmental pollution. The main chromium industries include metal plating and finishing, leather and textile manufacturing, electro-painting industries which discharge huge quantities of toxic metal ions to the surrounding environment [1–3]. Being non-degradable, chromium gets accumulated and persists in nature for a long time and may enter into the food chain causing remarkable health damage.

Chromium has been ranked as 17th among the most hazardous substances according to the Agency for Toxic Substances and Disease Registry (ATSDR) USA, 2017 [4]. Chromium occurs in different valency states, but stable states of chromium in the environment are Cr(VI) and Cr(III). Mining and industrial activities are the major sources of hexavalent chromium (VI) in the environment. Chromium (VI) is toxic to all forms of living systems including microorganisms which cause oxidative stress, DNA damage, and altered gene expression. Besides, Cr(VI) has been found to exhibit carcinogenicity, teratogenicity, and mutagenicity. Cr(VI) exposure in the environment causes serious health problems such as skin allergies, vomiting, diarrhea, brain damage, and premature death in mammals

as well as in plants it causes metabolic alterations, poor seed germination, stunted root growth, photosynthetic impairment, and death [5]. On the other hand, the trivalent chromium, Cr(III) is less toxic and relatively stable in the environment. Therefore, a reduction of Cr(VI) to Cr(III) is an immediate measure to undertake for the bioremediation of hexavalent chromium and reduce environmental pollution [6, 7].

Several reports have shown the characteristics of microorganisms and their enzymes in the biological reduction of Cr(VI) from different contaminated sources [8]. The biological reduction of Cr(VI) to less toxic Cr(III) has been considered to be one of the most practical and useful methods [9, 10]. The detailed Cr(VI) reduction mechanism has been elaborated by different groups of microorganisms, and the potential of the enzyme chromate reductases in bioremediation of Cr(VI) has also been investigated [11]. As compared to physicochemical and other treatments, biological reduction of Cr(VI) is an economical and environmentally friendly process. However, chromium bioremediation is a challenging task as Cr(VI) remains at a high concentration in groundwater and deeper soil [12]. Another ultimatum in the way of chromium bioremediation is that the Cr(VI) can easily disperse through the cell membrane with high solubility. A variety of Cr-resistant bacteria with high Cr(VI)-reducing potential have been reported to reduce Cr (VI) to Cr (III) which include *Pseudomonas*, *Bacillus*, *Enterobacter*, *Deinococcus*, *Shewanella*, *Agrobacterium*, *Escherichia*, *Thermus*, and many other species; thus, reduction by these enzymes affords a means of chromate bioremediation [13, 14]. The enzyme chromate reductase participates in the transfer of electrons during the reduction process and is an important candidate for bioremediation program [15].

Some chromate reductases alternatively called FMN reductases like nfrA2 from *Bacillus subtilis* are also able to reduce chromate [16, 17]. This class of enzyme reduces $FMNH_2$ to FMN, with the help of NADH or NADPH as reductant as well as also can reduce nitroaromatic compounds (hydroxybenzaldehyde), quinones, chromates, and azo dyes. FMN plays important role in binding with the active site in the enzymes of the chromate reductase family such as FMN reductase, N-ethylmaleimide reductase, and quinone reductase. FMN remains mainly involved in the reduction of Cr(VI) to Cr(III) through electronic transmission from NADPH to Cr(VI) [18, 19].

Enzymes and its activity can be investigated in a simple manner and in a shorter time with the help of In silico study, whereas experimental techniques are laborious, time-consuming, and also demand sophisticated and expensive infrastructures [20]. In silico structure-based study of proteins has now been widely and most frequently used in modern scientific world along with both the in vitro and in vivo experimental works. In this view to understand the mechanism by which FMN-dependent chromate reductases efficiently reduce toxic environmental chromium contaminants, different standard in silico approaches have been performed for a class of various bacterial chromate reductase-related enzymes. Sequence conservativeness in substrate (FMN) binding sites and phylogeny interrelationship have been determined for those enzymes. Three-dimensional structures of enzymes are crucial for understanding the correlation between their structure and function. Homology modeling was applied for the 3D structure prediction, important domains, and motifs analysis for different chromate reductase-related enzymes. Computer-based molecular docking is an important method to determine the interaction between enzymes and substrate and evaluate the binding modes and energy of the enzyme–substrate complex [21, 22]. In the current study, molecular interaction between different chromate reductase-related enzymes and FMN was determined along with their binding energy based on the complex prepared from molecular docking. For more detailed and in-depth understanding of protein's structure, function, and its actual reaction mechanism in real-time dynamical condition, a semi-empirical technique called molecular dynamics simulations (MDS) has now been mostly used. Therefore, in the current study, MDS has been performed to investigate comparative dynamics behavior and the stability of the wild-type and mutant quinone reductase from *E. coli* during the interaction with FMN. The study of this structural and dynamic aspect

Table 1 Template selected for homology modeling of different bacterial chromate reductase-related enzymes

Uniprot ID	Enzyme name	Organism name	Protein sequence length	Reference template selected for model building (PDB ID)
P0AGE7	Quinone reductase	*Escherichia coli*	188	IVYR
Q88FF8	Quinone reductase	*Pseudomonas putida*	186	3SVL
P0AGE8	Quinone reductase	*Shigella flexneri*	188	2Q62
P77258	N-ethylmaleimide reductase	*Escherichia coli*	365	3U7R
P74312	Quinone reductase	*Synechocystis sp*	206	3SVL

would help in designing more potent chromate reductase-related enzymes in the future which could have effective use in the reduction of environmental chromate pollution.

2 Materials and methods

2.1 Comparative sequence alignment and molecular modeling

Five amino acid sequences of bacterial chromate reductase-related enzymes have been taken from UniprotKB database (https://www.uniprot.org/). These amino sequences of these enzymes were selected based on the status as reviewed (high quality manually annotated) and also their crystal structures have not been solved yet; therefore, these protein sequences were taken for predicting their three-dimensional structure. All the retrieved sequences of the chromate reductase-related enzymes have been taken for comparative sequence alignment in Multalin server [23]. The sequence of quinone reductase from *E. coli* (Uniprot ID: P0AGE6) has been used as a reference to study the sequence conservativeness of flavin mononucleotide (FMN) binding site as the sequence has solved crystal structure bound with the ligand FMN [24]. For the molecular modeling and identification of FMN binding site in different bacterial chromate reductase-related enzyme, we have used existing crystal structure as the reference obtained from BLAST search and based on the highest sequence similarity the template structure has been chosen as a reference for individual sequence [25] (Table 1). All the chromate reductase-related enzymes have been modeled using the fold recognition server, Phyre2 [26]. All the modeled structures were energy minimized using steepest descent algorithm to obtain the lowest energy and stable conformation in NOMAD-REF server [27]. The quality of the models of different enzymes has been evaluated using PROCHECK [28] in terms of Ramachandran plot. ERRAT [29] was used to verify patterns of non-bonded atomic interactions and VERIFY3D [30] for assessing the compatibility of each amino acid residue in their favorable positions.

2.2 Protein–ligand interactions study

Knowledge-based docking approach has been undertaken to make the protein–ligand complex by using the binding grid of flavin mononucleotide (FMN) from the quinone reductase (YieF) bound reference structure from *E. coli* (PDB ID: 3SVL) [31] in Autodock Vina [32]. For the mutational study, the Asn85 residue present in the YieF of *E. coli* was mutated with tyrosine residue using *in-silico* residue mutation technique. The resultant docked complex was refined using Crystallographic Object-Oriented Toolkit (COOT) [33]. In addition with these modeled structures, we have also analyzed the structures of five other bacterial chromate reductase-related enzymes retrieved from the BRENDA database [34]. The molecular interaction of cofactors like FMN and FAD with these enzymes has also been studied. For visualization and analysis of the structural features and detecting substrate interactions, we have used COOT, PyMol [35], and Chimera [36]. Binding affinity between chromate reductase-related enzymes and FMN has been individually computed using a parallelized metadocking method implemented in the DINC server [37].

2.3 Functional domain identification and phylogenetic analysis

For the identification of protein families, domains, and functional sites in all the modeled and minimized enzymes, InterProScan tool was used [38]. For phylogenetic analysis of the modeled and FMN docked chromate reductase like enzyme, the amino acid sequences of those proteins have been deposited in the MEGA 7.1 software [39]. In the MEGA software, all the sequences were aligned pairwise firstly and then multiple basis using ClustalW. Phylogeny tree of the sequences was built using construct/test maximum likelihood (ML) statistical model which is based on nearest-neighbor-interchange (NNI) algorithm.

2.4 Molecular dynamics simulations

Two complex structures of *E. coli* ChrR in both its wild-type and Y85N mutant form bound with FMN were taken to perform MD simulation. All MD simulations were performed using the GROMACS 5.1.2 [40] and GROMOS96 43a1 force field [41] implemented on Intel Xeon Quad Core W3530 2.8 8 M 1366 Processor with LINUX environment. Both the complexes were solvated in a cubic box each with a dimension of 104.940 X 104.940 X 104.940 nm^3 containing 34,644 and 34,652 SPC216 water molecules [42]. All protein atoms were maintained at a distance of 1.0 nm from the box edges during the simulation. MD simulations of 100 ns were performed at 300 K temperatures for both the complex systems. Periodic boundary conditions were applied using Berendsen coupling algorithm to maintain the isothermal and isobaric conditions with a relaxation time of 0.1 and 0.2 ps, respectively [43]. To constrain the bond lengths of protein–ligand complexes, LINCS algorithm was used [44]. Electrostatic interactions of the complex systems were calculated using the particle mesh Ewald method, while the Van der Waals and coulombic interactions were calculated with a cutoff at 1.0 nm [45]. The tools provided by GROMACS program package were utilized to perform different analyses like RMSD, RMSF, Rg,

and SASA from MD trajectories. PyMOL and XMGrace [46] programs were used to analyze the results and to prepare figures from MD simulation. The covariance matrices of the positional fluctuations of Cα atoms during the dynamism of proteins were analyzed with PCA [47, 48].

3 Results and discussion

3.1 Comparative sequence alignment

To compare the differences between the retrieved chromate reductases sequences from NCBI and Uniprot database, multiple sequence alignment was performed. From the comparative sequence alignment between the chromate reductase-related enzymes from *E. coli, P. putida, S. flexneri, Synechocystis* sp., it has been observed that the FMN binding site Ser13 of *E.coli* (QR_Ec_POAGE6) is fully conserved in all the aligned sequences. Another FMN binding site, Arg15 of *E. coli* quinone reductase is shown to be conserved in all the compared sequences of chromate reductase-related enzyme except N-ethylmaleimide reductase of *E. coli* (NER_Ec_P77258). In NER_Ec_P77258, leucine is present in place of Arg15. As seen from the comparative sequence alignment, glycine is present in NER_Ec_P77258 in place of Ser18 of QR_Ec_POAGE6. However, Ser18 from QR_Ec_POAGE6 is shown to be conserved among the rest of the aligned bacterial chromate reductase-related enzymes. The cellulose binding residue, Phe19 of QR_Ec_POAGE6, has shown its conservativeness in quinone reductase of *E. coli* (QR_Ec_POAGE7) and *S. flexneri* (QR_Sf_P0AGE8). Multiple sequence alignments depicted the conservativeness of Asn20 of QR_Ec_POAGE6 among the quinone reductase of *E. coli* (QR_Ec_POAGE7), *P. putida* (QR_Pp_Q88FF8), and *S. flexneri* (QR_Sf_P0AGE8). NER_Ec_P77258 and NQR_Ssp_P74312 have been reported to retain arginine and serine, respectively, in place of Asn20 of QR_Ec_POAGE6. The FMN binding site, Glu82 of QR_Ec_POAGE6 found to be fully conserved in QR_Ec_POAGE7, QR_Pp_Q88FF8, QR_Sf_P0AGE8, and NQR_Ssp_P74312. NER_Ec_P77258 is only differed according to the conservativeness of Glu82 in QR_Ec_POAGE6 as it contains Serine in that place. The FMN interacting residues of QR_Ec_POAGE6, namely Tyr83, Asn84, and Ser117 are shown to be conserved in QR_Ec_POAGE7, QR_Ec_POAGE6, and QR_Sf_P0AGE8. Comparative sequence alignment revealed the presence of serine and methionine in NER_Ec_P77258 and NQR_Ssp_P74312, respectively, in place of Tyr83 of QR_Ec_POAGE6. In the case of NQR_Ssp_P74312, histidine is present in place of Asn84 in QR_Ec_POAGE6. In place of Tyr85 of QR_Ec_POAGE6, arginine, histidine, and glycine were found to be present in QR_Pp_Q88FF8, NER_Ec_P77258, and NQR_Ssp_P74312, respectively. Both the NER_Ec_P77258 and NQR_Ssp_P74312 were reported to contain valine in place of Ser117 of QR_Ec_POAGE6. It can be concluded from the result obtained from overall comparative sequence alignment that Ser13, Arg15, Ser18, Asn20, Glu82, and Asn84 (according to QR_Ec_POAGE6) remain conserved among most of the bacterial chromate reductase enzyme; hence, these conserved residues might have an important role in FMN binding and oxidoreductase activity of the enzyme (Fig. 1, Table 2). In a similar type of study conducted by Deng et al. [49], where comparative sequence alignment revealed that the amino acid sequence of FMN_red from *Serratia* sp. CQMUS2 has 99 and 94% identity to the enzymes from *Klebsiella pneumonia* and *Raoultella ornithinolytica*, respectively. In addition, their study also reported about the conservativeness of some residues, Tyr128, Glu146, Arg125, and Tyr85 which are associated with forming hydrogen bond networks to play a critical role in enhanced chromate reductase activity [49].

From the sequence alignment, it can be seen that the FMN binding residues are mostly conserved in the ChrR from *Gluconacetobacter hansenii* and *P. putida,* FerB from *Paracoccus denitrificans,* and YieF from *E. coli*. Most interestingly, ChrR from *Thermus scotoductus* and NemA from *E. coli* share more number of common FMN binding residues. NemA from *E. coli* has an FMN binding site ^{182}HSAH^{185} which is nearly conserved in ChrR from *T. scotoductus* where the sequence of FMN binding site is ^{172}HMAH^{175} (Fig. S1). The patches of conserved sequence in *T. scotoductus* ^{172}HMAH^{175} seem to play important role in the structural stability of the enzyme which is also deduced by the experimental study of Opperman and Heerden [50]. It was reported that the enzyme remains stable as well as active at a pH of 6.5 and temperature 65 °C with a Km and Vmax value of 55.5 ± 4.2 µM and a 2.3 ± 0.1 µmol Cr(VI) min^{-1} mg^{-1} protein, respectively [50].

3.2 Phylogenetic analysis

According to phylogeny analysis, chromate reductase from *Synechocystis* sp. is closely related to the chromate reductase enzyme from *Bifidobacterium moukalabense* and *Bifidobacterium* subsp. Oxygen-insensitive NADPH nitroreductase of *E. coli* and FMN reductase of *B. subtilis* are the two enzymes shown to be distantly related to the chromate reductase from *Synechocystis* sp. Chromate reductase of *Synechocystis* sp. is also related to the outgroup N-ethylmaleimide reductase and chromate resistance protein from *E. coli* and *Candidatus Jettenia caeni*, respectively. According to the sequence homology of N-ethylmaleimide reductase of *E. coli* with all other aligned chromate reductase-related enzyme from other organisms, it was shown that the chromate resistance

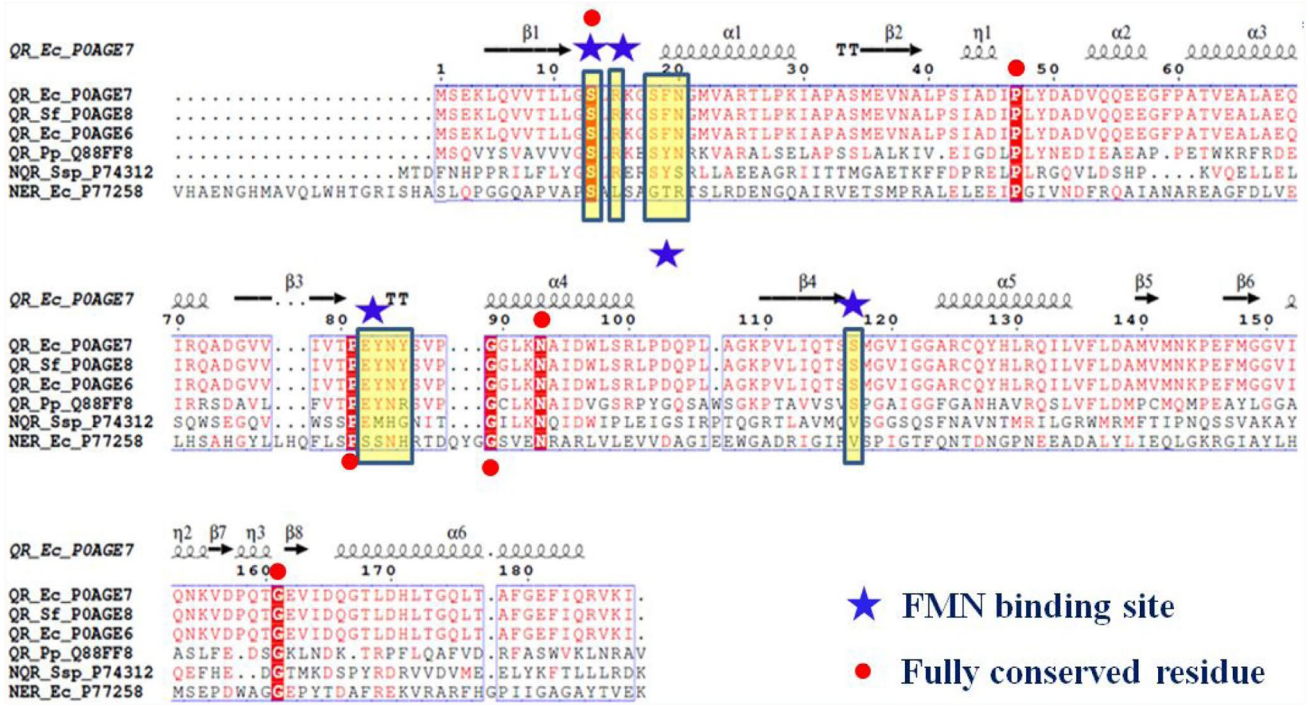

Fig. 1 Comparative sequence conservativeness analysis in FMN binding site of different bacterial chromate reductase-related enzymes

Table 2 FMN binding sites in different bacterial chromate reductase-related enzyme

Enzyme name	FMN binding sites									
QR_Ec_ P0AGE6	Ser13	Arg15	Ser18	Phe19	Asn20	Glu82	Tyr83	Asn84	Tyr85	Ser117
QR_Ec_ P0AGE7	Ser13	Arg15	Ser18	Phe19	Asn20	Glu82	Tyr83	Asn84	Tyr85	Ser117
QR_Pp_ Q88FF8	Ser13	Arg15	Ser18	Tyr19	Asn20	Glu80	Tyr81	Asn82	Arg83	Ser116
QR_Sf_ P0AGE8	Ser12	Arg14	Ser17	Phe18	Asn19	Glu81	Tyr82	Asn83	Tyr84	Ser116
NER_Ec_P77258	Ser124	Leu126	Gly129	Thr130	Arg131	Ser196	Ser197	Asn198	His199	Val235
NQR_Ssp_P74312	Ser16	Arg18	Ser21	Tyr22	Ser23	Glu81	Met82	His83	Gly84	Val117

*Yellow highlighted residues are mostly conserved in all types of bacterial chromate reductase-related enzymes

protein of *Candidatus jettenia* is in close proximity with *E. coli* N-ethylmaleimide reductase. Quinone reductase of *P. putida* is evolutionary belongs to the in-group consortia of *Pseudomonas* sp. N-ethylmaleimide reductase, *P. japonica* chromate reductase, and *P. simiae* chromate reductase. Quinone reductase of *E. coli* and *S. flexneri* is evolved under the same evolutionary branch with *E. fergusonii* chromate reductase (Fig. 2). Like this analysis, Deng et al. [49] constructed a phylogenetic tree of the FMN_red members, including ChrT using the neighbor-joining method with MEGA software [49]. According to the phylogenetic tree deduced from this study, ChrT was found to be closely associated with FMN_red members from the bacteria including *K. pneumonia, R. ornithinolytica,* and *K. oxytoca.*

3.3 Structures of chromate reductase family enzymes from different bacterial species

From the three dimension structure prediction, it can be shown that all the modeled chromate reductases like enzymes of different bacterial species have a similar type of α/β secondary content. Results from the molecular docking study of all these chromate reductase like enzymes with the substrate, FMN revealed that the binding sites of the cofactor (FMN) are position towards the surface of the protein. There is significant similarity in the overall three-dimensional structure of chromate reductase-related enzymes from *Synechocystis* sp, *E. coli*, *P. putida*, and *S. flexneri*, whereas N-ethylmaleimide

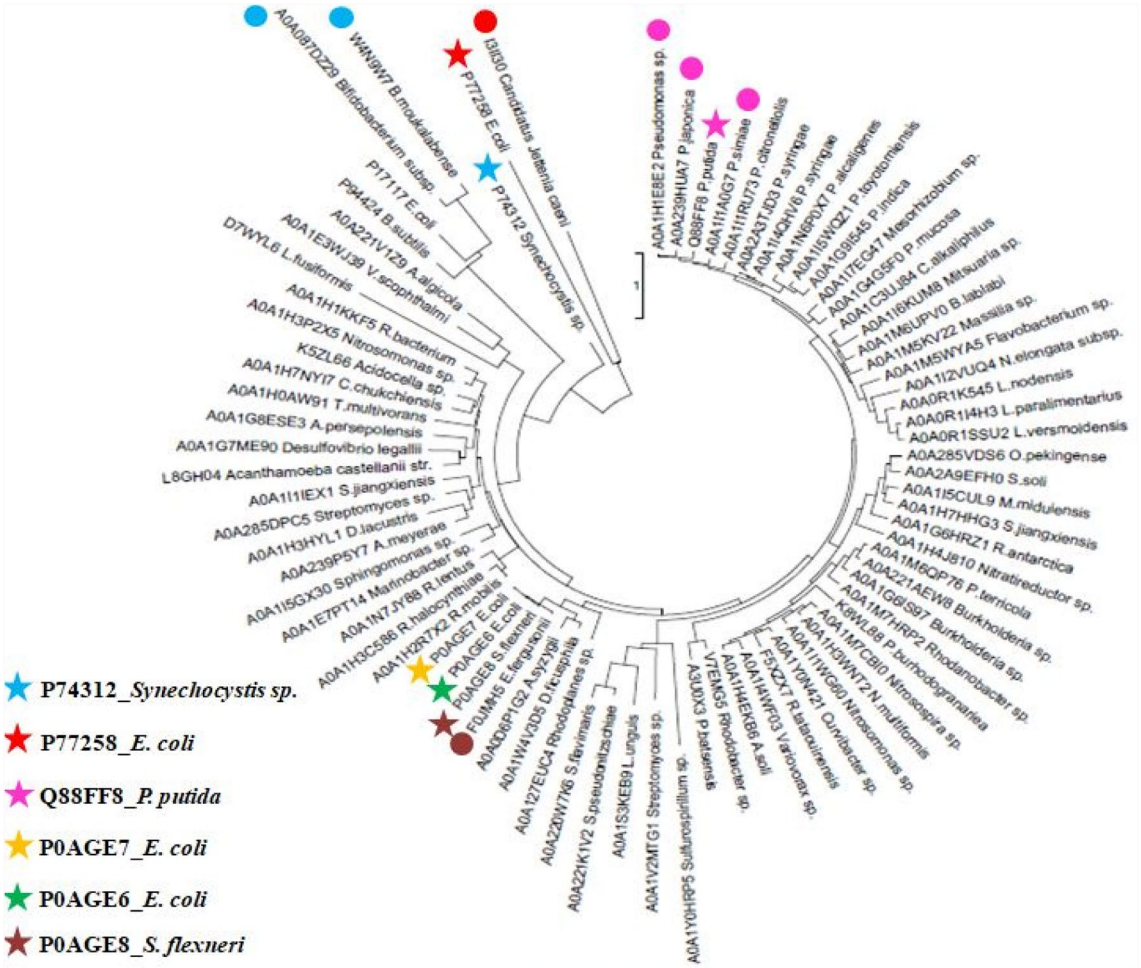

Fig. 2 Phylogenetic tree of the modeled bacterial chromate reductase-related enzyme

reductase of *E. coli* has a typical aldolase-type TIM barrel structure. Electrostatic potential surface analysis of all the chromate reductase like enzymes bound with FMN suggested that there is notable diversity in the chemical environment of the substrate binding groove in each of the complex modeled system. In the case of quinone reductase of *Synechocystis* sp., the amine group (-NH) containing dioxobenzo[g]pteridin moiety of FMN shown to be placed within a hydrophobic patch, whereas the 7,8-dimethyl attached dioxobenzo[g]pteridin moiety of FMN is shown to be positioned within a groove enriched in positively charged amino acids. The phosphate group containing chain of FMN remains packed under a pocket consist of positively charged amino acids (Fig. 3).

Riboflavin ring of FMN is shown to be placed comparatively more hydrophobic cleft in the quinone reductase of *E. coli*. The phosphate group containing chain of FMN is also placed under a binding groove consists of positively charged amino acids. Likewise, in the case of quinone reductase of *Synechocystis* sp., the amine group (-NH) containing dioxobenzo[g]pteridin moiety of FMN is also shown to be positioned inside a patch of negatively charged amino acids in *P. putida* quinone reductase. The 7,8-dimethyl attached dioxobenzo[g]pteridin moiety of FMN has been noted to be situated inside a hydrophobic patch of the enzyme. The phosphate group of the ligand FMN reported to interact with the residues under a negatively charged canal of the enzyme (Fig. 3).

The FMN binding site in N-ethylmaleimide reductase of *E. coli* is significantly differed from the binding site of FMN found in other complexed models. Electrostatic surface of FMN binding site in these enzymes reveals that the ligand extensively interacts with the residues that are hydrophobic in nature. In the quinone reductase of *S. flexneri*, the 7,8-dimethyl attached dioxobenzo[g]pteridin moiety of FMN is shown to be placed within a binding pocket consist of a combination with both the hydrophobic and positively charged residues. The phosphate group of the ligand

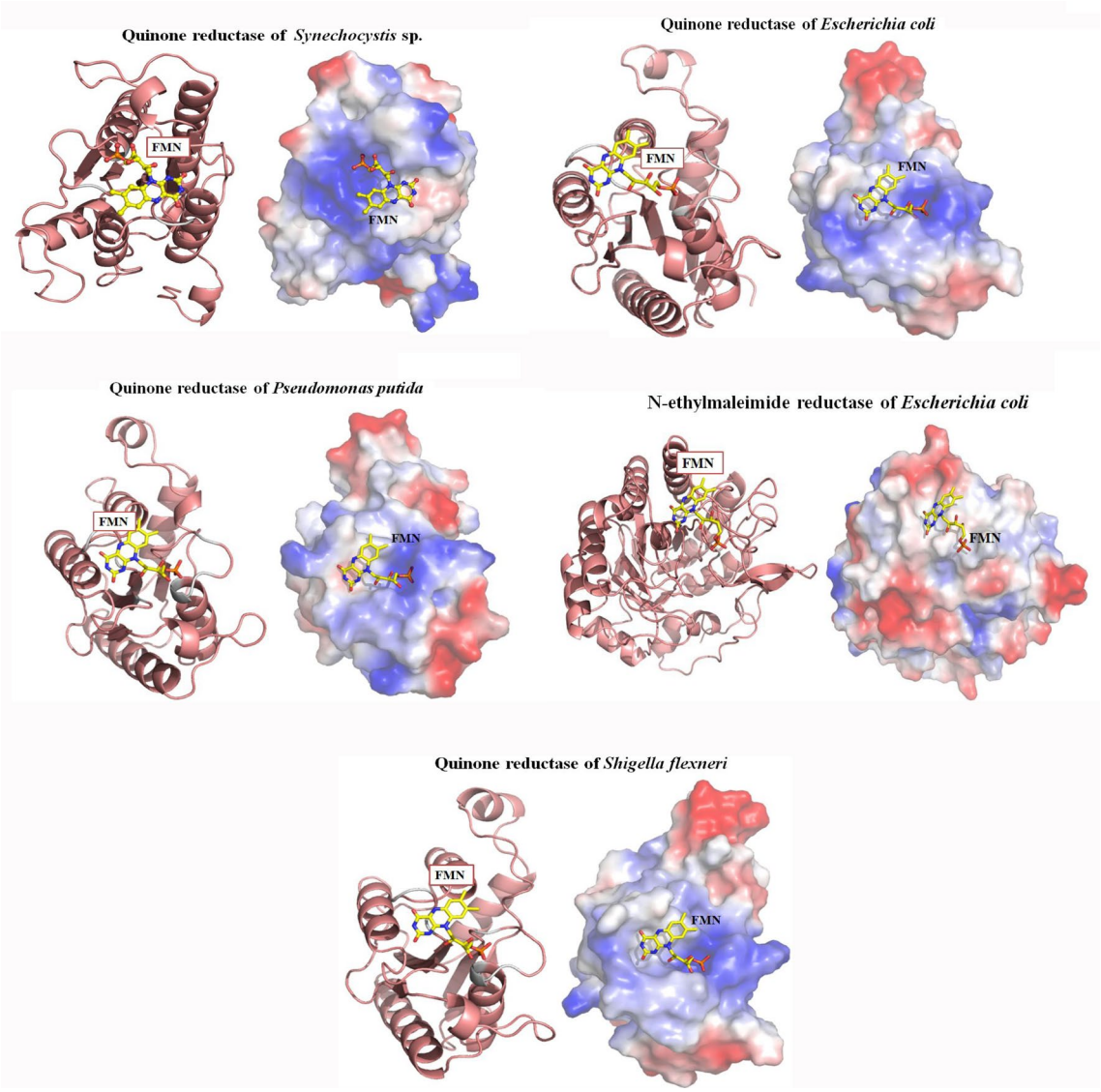

Fig. 3 Cartoon (left) and electrostatic potential surface (right) representation of FMN bound chromate reductase like enzymes

is shown to be inserted under a groove assembled with positively charged amino acids (Fig. 3). Structural analysis of the enzymes as conducted in the present study is similar to the work of Deng et al. [49] where they predicted the 3-D structure of ChrT using the SWISS-MODEL program based on a known crystal structure of the *E. coli* ChrR enzyme. From the structural analysis of ChrT protein, it was shown that the protein contains 40.96% α-helix, 11.70% extended β-strand, and 47.34% random coil [49].

The structures of five other chromate reductase like enzymes from different bacterial species have been retrieved and analyzed in the current study (Fig. S2). From the structural analysis, it can be shown that all the enzymes have a common α/β secondary structure contents as we have found in the above described all the modeled chromate reductase like enzymes. Among these five structures, a typical α/β TIM barrel structural motif has been found in the case of tryptophan repressor binding protein WrbA from *Deinococcus radiodurans* (PDB ID: 1YRH) [51] (Fig. S2(a)) and the old yellow enzyme (OYE) from *T. scotoductus* (PDB ID: 3HF3) (Fig. S2(c)) [52]. But for the rest of the structures, the β-sheets are shown to be in a dispersed position and rather found adjacent towards the surface of proteins (Fig. S2(e,g,i)). Comparative analysis of all the structures of these five different chromate reductase like enzymes reveals the presence of different folds in their three-dimensional conformation. The phosphate moiety of the cofactor FMN is shown to retain common binding motifs in the WrbA from *D. radiodurans* (Fig. S2(b)) and chromate/uranium reductase of *G. hansenii* (PDB ID:

3S2Y) (Fig. S2(f)) [18] which is mostly composed of serine residues as found in the previously described modeled structures of quinone reductase of *E. coli*, *P. putida*, and *S. flexneri*. Significantly different binding sites have been reported in the case of FAD interaction with the enzyme NADPH-specific quinone oxidoreductase (Smu. 1420) from *Streptococcus mutans* UA159 (PDB ID: 3LCM). The binding site of FAD in the enzyme Smu. 1420 reported containing residues, namely His9, Phe15, Asn16, Ile83, Trp85, Ser86, Thr130, Tyr141, and Arg174 (Fig. S2(j)) [53].

WrbA from *D. radiodurans* reported to belong from the flavodoxin family of enzyme and was recognized as the first enzyme classified under this family [51]. The OYE from *T. scotoductus* along with its characteristics α/β TIM barrel structure is also shown to contain a capping domain that is constructed by two small antiparallel β-sheets. This capping domain was reported being responsible for channeling the cofactor FMN inside the active site during the enzymatic catalysis and also might have some role in the thermal stabilization of the enzyme [52]. WrbA-related protein A (WrpA) from *Brucella abortus* (PDB ID: 5F4B) has been reported to be classified under the flavodoxin family [54]. In case of WrpA from *B. abortus*, FMN shown to be bound at the outer surface of the enzyme has only retained a single bonding interaction with the residue His134 (Fig. S2(h)).

3.4 Model validation of different chromate reductase-related enzymes

Ramachandran plot analysis of the modeled quinone reductase of *Synechocystis* sp. depicted that 82.9% residues are in most favor region which is responsible for the construction of most compact secondary structure contents like α- helix and β-sheets. 14.9% residues from the total amino acid sequence of *Synechocystis* sp. quinone reductase are in additional allowed regions that form 3^{10} helices, β-turned, and loops. In the case of quinone reductase of *E. coli*, 84.1% of residues are in the most favored regions of the Ramachandran plot derived from the model validation. An additional allowed region in the predicted structure of this enzyme contains 13.4% residues. Modeled quinone reductase of *P. putida* has 81.1% residues in most favor region, while 15.7% amino acid is in additional allowed regions. N-ethykmaleimide reductase of *E. coli* retains 80.3% residues belong to the most favored region and 18.0% of the residues from additional allowed regions. Ramachandran plot depicted that the modeled quinone reductase of *S. flexneri* has 83.1% of residues plotted inside most favored regions, whereas 14.3% residues are from the additional allowed regions (Fig. S3).

3.5 Functional domains, motifs, and active site in different chromate reductase-related enzyme

Different types of domains and motifs have been identified in the modeled chromate reductase-related enzymes from the analysis by InterProscan server. Quinone reductase enzymes of *Synechosystis* sp. are shown to have three different domains called flavoprotein like superfamily domain, NADPH-dependent FMN reductase like domain, and arsenate resistance (ArsH) domain which range within the amino acids numbering from 1–205, 8–151, and 1–204, respectively. N-ethylmaleimide reductase from *E. coli* reported containing aldolase-type TIM barrel and NADH-flavin oxidoreductase/NADH oxidase, N-terminal domain. The residue number from 4–350 belonged to the aldolase-type TIM barrel. NADH-flavin oxidoreductase/NADH oxidase, N-terminal domain of this enzyme is constructed by the residues ranges from 5 to 338. Quinone reductases of *E. coli, S. flexneri*, and *P. putida* share domains that are common between them. These domains are called Flavoprotein like superfamily domain and NADPH-dependent FMN reductase like domain. The length of these two domains in the quinone reductase of *E. coli* and *S. flexneri* is exactly the same, which is 1–188 and 6–148 for flavoprotein like superfamily and NADPH-dependent FMN reductase like domain, respectively. Quinone reductase of *P. putida* has these two domains ranges from 6–185 and 7–149 residues (Fig. 4). Ball et al. [55] annotated the functional domains of nitronate monoxygenase which reveals a new class of NADH dependent quinone reductases from *P. aeruginosa* PAO1. Six conserved motifs from these enzymes have been identified which defines a new class of NADH dependent quinone reductases. Among these six, motifs I and V are reported to have possible binding efficacy with the cofactor and modulate the redox potential. Motif II and Motif III both are reported to be a part of the TIM barrel domain [55]. Thus, it can be concluded from the current study and the work done by Ball et al. [55] that the TIM barrel domain and its fold along with the motifs I, II, III, and V of quinone reductase enzyme classes have an important role in structural stability and enzymatic activity.

3.6 Molecular interactions of different bacterial chromate reductase-related enzymes with FMN

Molecular interaction study from the docked complex presented that the side-chain OG atom of Ser16 in quinone reductase of *Synechocystis* sp. makes bonded interaction with the O3P atom of the phosphate group in the bound ligand flavin mononucleotide (FMN) with a bond distance of 3.32 Å. The O2P atom of this ligand phosphate moiety is shown to remain bound with the side-chain OG atom and main-chain nitrogen of Ser23 of the enzyme with a bond

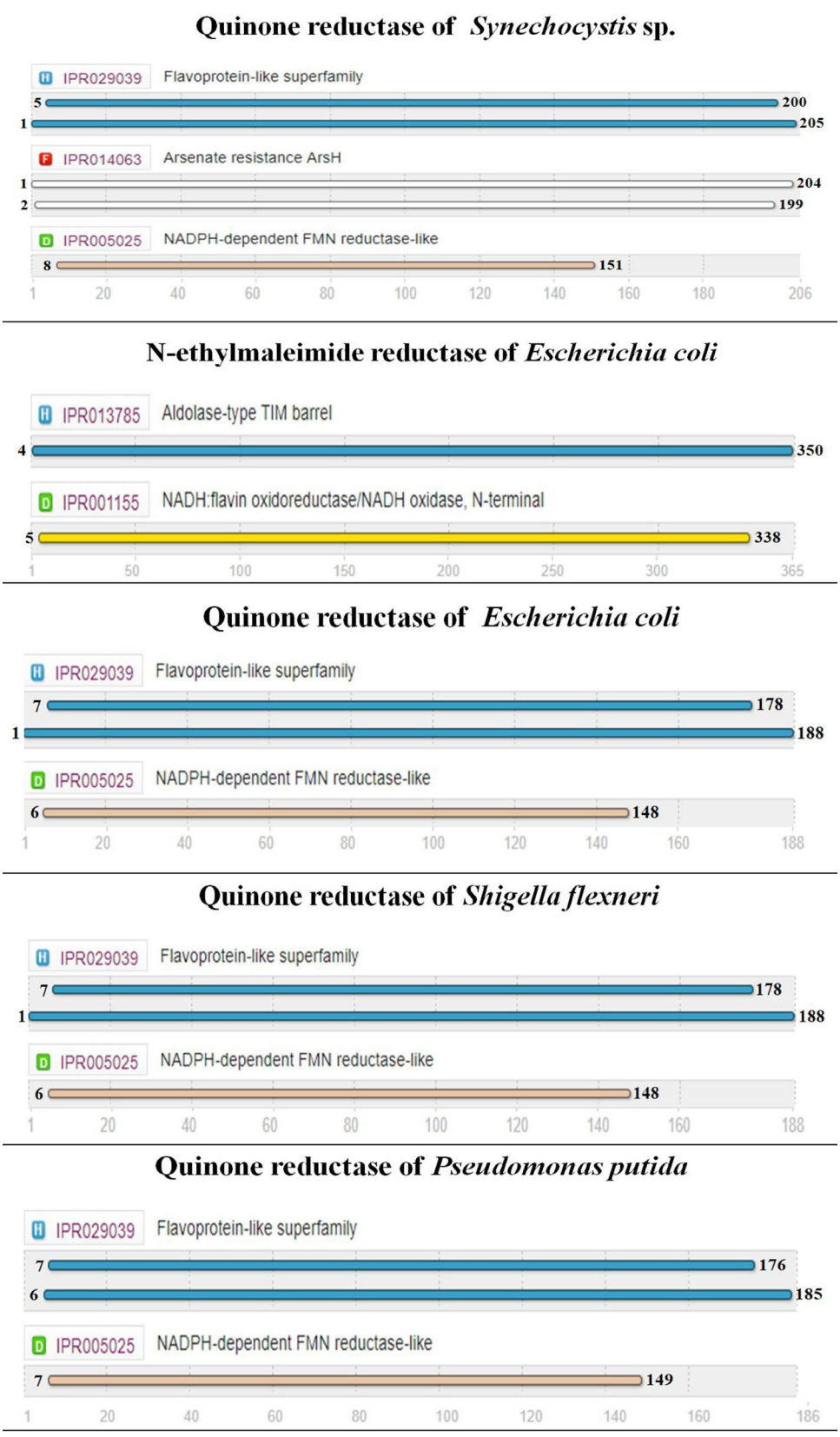

Fig. 4 Functional domains and motifs in different bacterial chromate reductase like enzymes

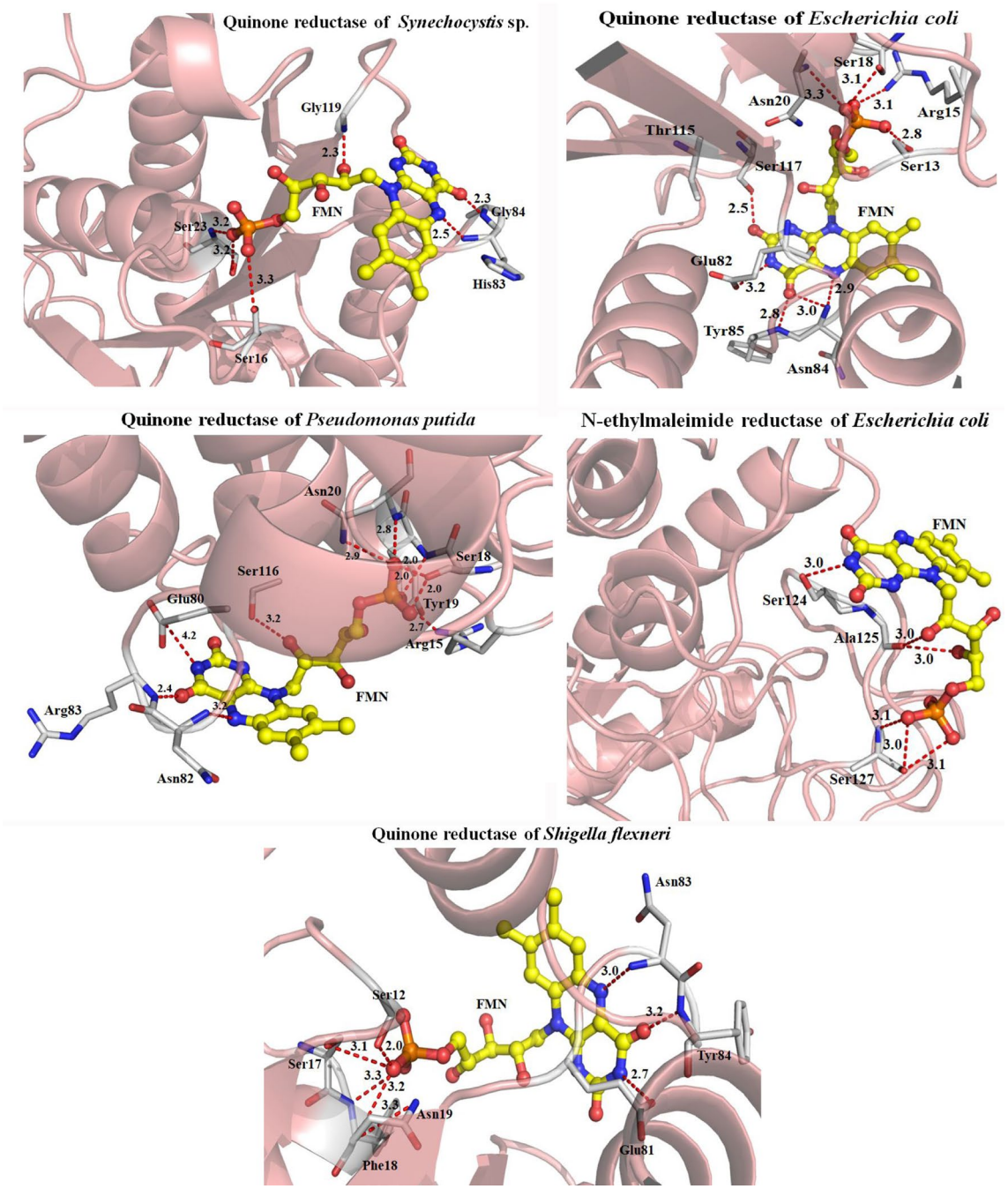

Fig. 5 Molecular interaction of the substrate FMN with differet chromate reductase like enzyme

length of 3.24 and 2.25 Å, respectively. The main-chain nitrogen atoms from His83 and Gly84 of this enzyme are shown to interact with one of the nitrogen of the central hexane ring and O4 atom of the dioxobenzo[g]pteridin ring of flavin mononucleotide with a distance of 2.5 and 2.3 Å, respectively (Fig. 5, Table 3). The main-chain nitrogen atom of Gly119 of the same enzyme remains connected with the O2 atom of the ester chain of FMN that connects the flavin mononucleotide with the phosphate group. There are some hydrophobic contributions in the FMN binding site from the residues Arg18, Ser21, Tyr22, Pro80, Glu81, Met82, Val11, Ser118, and Ala151 of *Synechocystis* sp. quinone reductase (Table 3).

Analyzing the molecular interaction of N-ethylmaeimide reductase from *E. coli*, it has been found that the side-chain OG atom of Ser124 residue interacts with the N3 atom of the dioxobenzo[g]pteridin moiety of flavin mononucleotide head region with a bonding distance of 3.0 Å.

Table 3 Molecular interactions and bond distances between the protein and ligand atom of the modeled complex between different bacterial chromate reductase like enzymes with FMN

Protein atoms	Ligand atoms	Distance	Residues involved in hydrophobic interaction
Quinone reductase of *Synechocystis* sp.			
Ser16OG	O3P	3.32	Arg18,Ser21,Tyr22,Pro80,Glu81,Met82,Val11, Ser118, Ala151
Ser23OG	O2P	3.24	
Ser23N	O2P	2.25	
His83N	N5	2.51	
Gly84N	O4	2.29	
Gly119N	O2	2.31	
N-ethylmaleimide reductase of *Escherichia coli*			
Ser124OG	N3	3.00	Leu126, Met148, Ala151, Glu153, His199
Ala125O	O4	3.02	
Ala125O	O2	2.99	
Ser127OG	O3P	3.04	
Ser127N	O3P	3.06	
Ser127OG	O2P	3.09	
Quinone reductase of *Pseudomonas putida*			
Ser13OG	O3P	2.20	Pro79, Tyr81, Pro117, Ile120
Arg15NH1	O1P	2.73	
Ser18OG	O2P	2.01	
Ser18OG	O3P	2.04	
Tyr19N	O1P	2.79	
Asn20N	O2P	2.83	
Asn20ND2	O2P	2.91	
Glu80OE1	N3	4.16	
Asn82N	N5	3.17	
Arg83N	O4	2.35	
Ser116OG	O2	3.24	
Ser116OG	O2	2.80	
Quinone reductase of *Escherichia coli*			
Ser13OG	O3P	3.10	Phe19,Pro81,Tyr83,Met118
Arg15NH1	O1P	2.77	
Ser18OG	O2P	3.11	
Asn20N	O2P	3.27	
Glu82OE2	N3	3.20	
Asn84N	N5	2.90	
Asn84N	O4	3.02	
Tyr85N	O4	2.75	
Ser117OG	O2	2.53	
Quinone reductase of *Shigella flexneri*			
Ser12OG	O2P	2.04	Arg14,Pro80,Tyr82,Ser116,Met117
Ser17OG	O2P	3.33	
Phe18N	O1P	3.19	
Asn19N	O2P	3.13	
Asn19 ND2	O2P	2.33	
Glu81OE2	N3	3.22	
Asn83N	N5	3.00	
Tyr84N	O4	2.66	

Both the oxygen atoms (O2 and O4) of the linker ester chain between the flavin mononucleotide head group and phosphate moiety make their interactions with the main-chain oxygen atom of Ala125 with an interaction lengths of 2.99 and 3.02 Å, respectively (Fig. 5). Ser127 of this enzyme has been marked as an important residue that forms three bonds with the O3P and O2P atoms of the phosphate group of the ligand FMN. Side-chain OG groups of Ser127 make two bonds with O3P and O2P atom of the phosphate with the interacting distance of 3.04 and 3.09 Å, respectively (Fig. 5, Table 3). The main-chain nitrogen of this serine has interaction with the O3P atom of phosphate with a distance of 3.06 Å. The residues Leu126, Met148, Ala151, Glu153, and His199 make their hydrophobic contribution in the binding of FMN within the interacting pocket of the enzyme N-ethylmaeimide reductase of *E. coli*. It can be seen from the hydrophobic interaction analysis that the residue Leu126 is adjacent to the serine that is reported above as important for the phosphate group binding in ligand FMN. The hydrophobic contribution of Leu126 residue might have some regulatory role in the spatial arrangement of Ser127 in the binding site of FMN in this enzyme (Table 3).

From the comparative molecular interaction analysis of the five modeled complex of different bacterial chromate reductase like enzymes, it can be deduced that quinone reductase of *P. putida* possesses the most number of interactions with the ligand FMN. A total of 12 protein–ligand interactions have been listed here from the interaction analysis. The phosphate moiety of FMN is shown to be involved in 7 interactions out of these 12. O3P atom of phosphate makes two interactions with the side-chain OG of both Ser13 and Ser18 residues of the enzyme with a distance of 2.20 and 2.04 Å, respectively. O2P atom of phosphate group has three numbers of interactions with the side-chain OG of Ser18 and both the side-chain ND2 and main-chain nitrogen of Asn20 residue of the enzyme with a bond length of 2.01, 2.83, and 2.91 Å, respectively. There are two bonded interactions that have been reported between the O1P ligand atom each with the side-chain NH1 of Arg15 and nitrogen of Tyr19 with a bond distance of 2.73 and 2.79 Å, respectively (Fig. 5, Table 3). Side-chain OE1 atom present in Glu80 involves in the interaction with N3 atom of the dioxobenzo[g]pteridin moiety in flavin mononucleotide. The main-chain nitrogen of Asn82 remains bound to the N5 atom of the central hexane ring of the dioxobenzo[g]pteridin moiety of flavin head group with a bond length of 2.35 Å. Side-chain OG atom of Ser116 has two interactions with ligand FMN: one of them is with oxygen (O2) atom from the dioxobenzo[g] pteridin moiety of FMN head group and the other is with the oxygen (O2) atom from the ester chain with a bond distance of 2.8 and 3.24 Å, respectively (Fig. 5, Table 3). The residues of quinone reductase of *P. putida* shown to be involved in the hydrophobic interactions with ligand FMN are Pro79, Tyr81, Pro117, and Ile120 (Table 3). Among these residues, Pro79 seems to have some additional contribution to maintain the spatial arrangement of the side chain in Glu80 as these two residues are linked together by a peptide bond. Thus, Pro79 might be responsible for the proper positioning of the OE1 side-chain atom of Glu80 so that it can interact with the N3 atom present at the dioxobenzo[g]pteridin moiety of FMN.

Study of molecular interaction from the docked complex showed that quinone reductase of *E. coli* makes bonded interactions with the ligand FMN by the residues Ser13, Arg15, Ser18, Asn20, Glu82, Asn84, Tyr85, and Ser117. The phosphate group of FMN is shown to possess four interactions with the residues Ser13, Arg15, Ser18, and Asn20 of this enzyme. Side-chain OG of Ser13 is shown to interact with the O3P atom of the phosphate group in ligand. The O2P atom makes two interactions with the side-chain OG atom of Ser18 and the main-chain nitrogen of Asn20 with a bond distance of 3.11 and 3.27 Å, respectively (Fig. 5, Table 3). Side-chain NH1 atom of Arg15 has an interaction with the O1P atom of FMN phosphate with a bond length of 2.77 Å. N3 atom of the dioxobenzo[g]pteridin moiety from the FMN head group region forms a hydrogen bond with the side-chain OE2 of Glu82 with a distance of 3.20 Å. N5 atom of the middle hexane ring in the dioxobenzo[g]pteridin moiety is shown to interact with the main-chain nitrogen of Asn84. Both the main-chain nitrogen atoms of Asn84 and Tyr85 are shown to interact with the oxygen (O4) atom situated in the dioxobenzo[g]pteridin moiety in FMN head group. Side-chain OG atom of Ser117 makes a connection with the oxygen (O2) atom of the dioxobenzo[g]pteridin moiety in the ligand, FMN with a distance of 2.53 Å. Residues Phe19, Pro81, Tyr83, and Met118 are found to be important in providing hydrophobic interaction with the ligand FMN. All these residues are shown to be in close proximity with some of the FMN interacting amino acids like Ser18, Glu82, Asn84, and Ser117. Above-mentioned residues involved in hydrophobic interactions might be responsible for the proper positioning of the residues that makes bonded interactions with the ligand FMN as they have been reported to originate from the same structural patches in quinone reductase of *E. Coli* (Table 3).

In the study of Jin et al. [18], it has been found that the ligand FMN binds in a pocket of chromate reductase of *Gluconacetobacter hansenii* near the dimer interface of this enzyme. The FMN binding pocket in this enzyme is composed of the residues, namely Ser15, Arg17, Ser20, Phe21, Asn22, Glu83, Asn85, and Tyr86. The residues such as Tyr51, Pro82, Tyr84, Arg101, and Pro119 are reported to

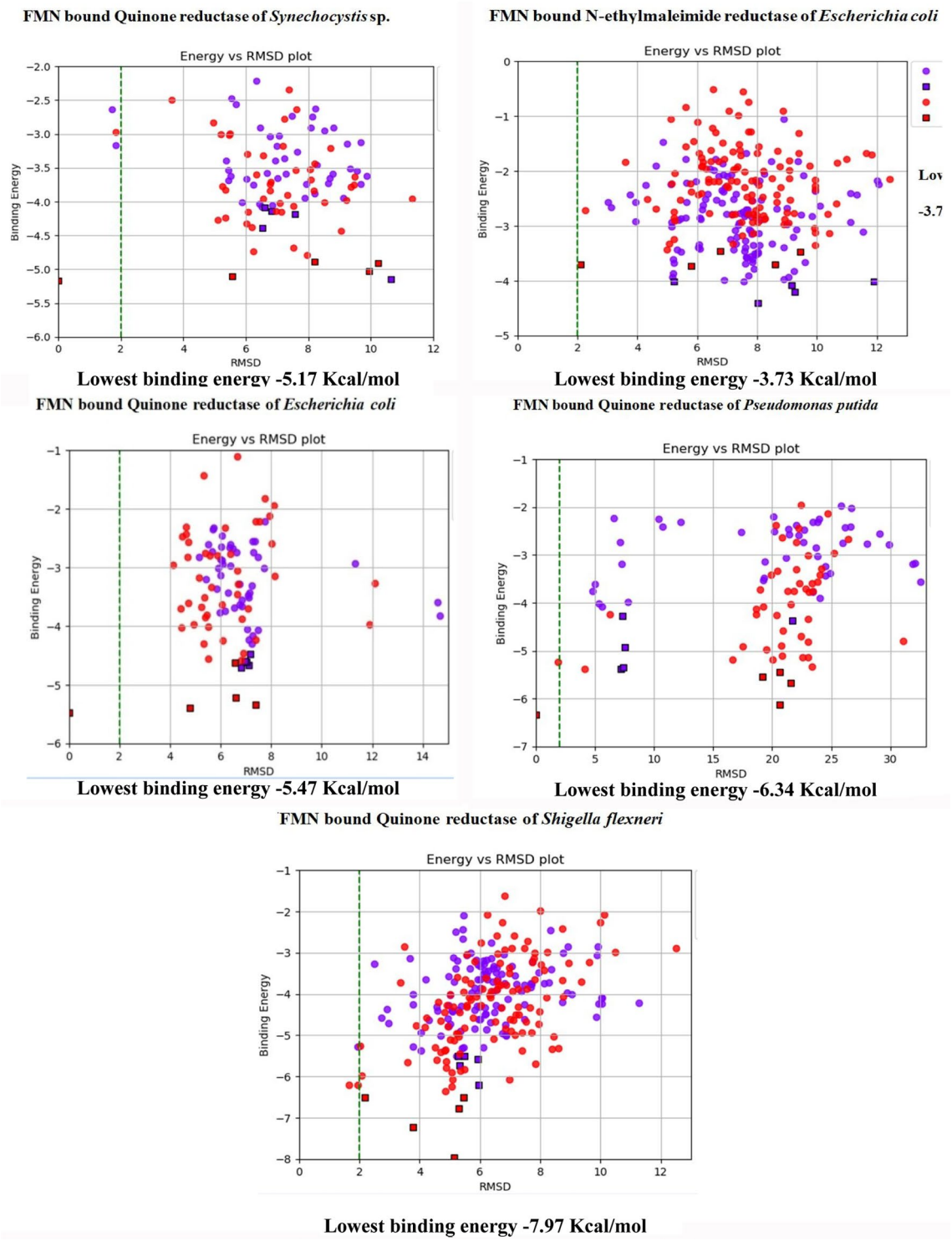

Fig. 6 Binding energy analysis of different bacterial chromate reductase family enzymes bound with the ligand flavin mononucleotide

contribute to the formations of hydrophobic interactions with the ligand FMN [18].

Analyzing the molecular interaction of quinone reductase from *S. flexneri* with its ligand FMN, it was found that both the side-chain OG atoms from Ser12 and Ser17 form interactions with the O2P atom of the ligand phosphate group with an interacting length of 2.04 and 3.33 Å. The same O2P atom of the ligand was also shown to interact

with the main-chain nitrogen from Asn19 with a bond distance of 3.13 Å. O1P atom of the phosphate moiety was reported forming interaction with the main-chain nitrogen of Phe18 with a bond length of 3.19 Å. Side-chain ND2 atom of Asn19 form a hydrogen bond with the O2P atom in the phosphate moiety within a distance between 2.33 Å. Glu81 of the enzyme shown to form interaction with the N3 atom in dioxobenzo[g]pteridin moiety of FMN head region by the side-chain OE2 within a distance of 3.22 Å. N5 atom from the middle hexane ring of the dioxobenzo[g]pteridin head group in flavin mononucleotide forms an interaction with the main-chain nitrogen of Asn83 with a range between 3 Å. The main-chain nitrogen of Tyr84 of this enzyme was found to involve in forming interaction with the O4 atom in dioxobenzo[g]pteridin moiety of FMN. The residues involved in hydrophobic interaction with the ligand FMN are reported as Arg14, Pro80, Tyr82, Ser116, and Met117. From these residues, Pro80 and Tyr82 are assumed to be important in the sense that they might have some impact in positioning their two adjacent residues Glu81 and Asn83 to come into the suitable spatial arrangement so that they can make interaction with the dioxobenzo[g]pteridin moiety of FMN. Pradhan et al. [56] in their reports have been presented about the molecular interaction between FMN with different bacterial chromate reductase family enzymes using proteomics and bioinformatic analysis like the studies undertaken in the current work.

Table 4 Chromate reductase activity of ChrR mutant enzymes

Enzyme	nM Cr(VI) reduced min^{-1} mg^{-1} protein	Enhancement factor
Chr wild type	860 ± 50	–
Chr Y85N	11,496 ± 134	13 times increase

3.7 Binding energy analysis

From the comparative binding energy analysis of the modeled bacterial chromate reductase family enzymes bound with the ligand flavin mononucleotide (FMN), it has been found that the highest ligand affinity of -7.97 kcal/mol is recorded for the quinone reductase enzyme from *S. flexneri*. Second highest binding affinity for the ligand has been reported for the enzyme quinone reductase of *P. putida* with a value of −6.34 kcal/mol. Quinone reductase from *Synechocystis* sp., *E. coli,* and N-ethylmaleimide reductase of *E. coli* has the binding energy with a value of −5.17, −5.47, and −3.73 kcal/mol, respectively, when they interact with the ligand, FMN (Fig. 6). Borshchevskiy et al. [57] in their study determined the noncovalent binding of free FMN to NADH dependent quinone oxidoreductase from *Vibrio harveyi* by isothermal titration calorimetry [57]. The observed effect was < < 0.1 kcal/mol of FMN (unpublished data), which is more than 100-fold lower comparing to FMN binding by flavoproteins [58, 59]. Reports from these previous studies along with our current study suggest that the enzyme quinone reductase can bind with different ligands with variable affinities.

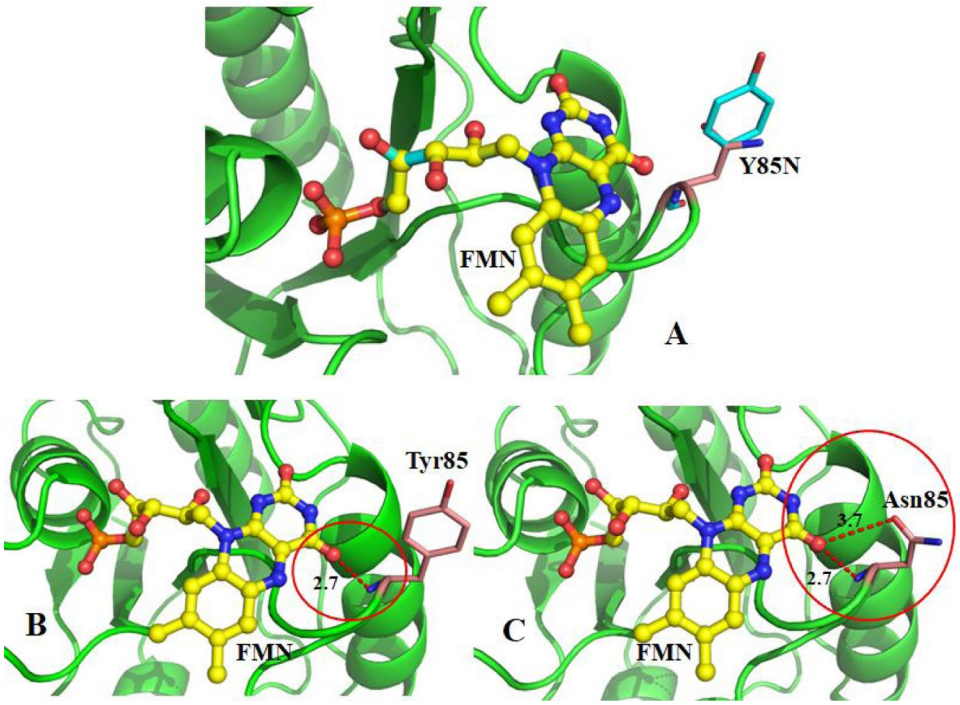

Fig. 7 Structure alignment of the FMN binding region of wild type and Y85N mutant of *E. coli* quinone reductase (A). Comparative molecular interactions of protein–ligand in two systems, wild type (left) and Y85N (right)

3.8 Mutation studies for optimum chromate reductase activity

In the modeled quinone reductase of *E. coli,* Tyr85 has shown to be crucial among the FMN binding residues. The main-chain nitrogen atom of Tyr85 makes an interaction with the oxygen atom which is adjacent -*meta* positioned with the terminal –NH group present in the dioxobenzo[g] pteridin of flavin nucleotide. Previous work has shown that substitution of this residue by asparagine in the mutant enzyme greatly improves chromate reductase activity of ChrR (Table 4) [31].

In the present study, increased chromate reductase activity in the Y85N mutant of *E. coli* quinone reductase enzyme has been investigated in light of the molecular mechanism responsible behind it. Difference in the molecular interactions was interpreted from aligning FMN bound complex structure of both the wild type and Y85N mutant of *E. coli* quinone reductase enzyme. In wild-type protein, main-chain nitrogen atom of Tyr85 was found to interact with one of the oxygen atom in the dioxobenzo[g] pteridin moiety of ligand FMN. Interestingly, in the case of Y85N mutant, there are two interactions reported to form between the main-chain nitrogen and the side-chain OE1 atom with the same oxygen atom of the ligand FMN (Fig. 7). This increased number of protein–ligand interactions might have some implications to fit the ligand FMN more firmly in its binding groove under the enzyme. This stronger binding of the ligand in Y85N mutant might address the cause of its enhanced chromate reducing efficacy than the wild type as already discussed in the experimental method.

In the present study, for an in-depth understanding of the overall dynamical aspect for the Y85N mutant of *E. coli* quinone reductase bound to FMN and the comparative structural stability with the wild-type form, MD simulation has been performed for both the wild type and Y85N mutant of *E. coli* quinone reductase complexed with FMN.

4 MD simulation

4.1 Root mean square deviation

According to RMSD analysis, it has been found that FMN bound wild-type *E. coli* quinone reductase has less residual backbone deviation compared to the Y85N mutant up to 7 ns timescale of MD simulation. After that, Y85N mutant quinone reductase of *E. coli* showed less RMSD value compared to the wild-type quinone reductase up to 50 ns of the MD simulation trajectory. Within a timescale during 50–55 ns of simulation, there is a sudden peak in the RMSD curve has been noticed for Y85N mutant which is even higher than the wild-type *E. coli* quinone reductase. But after 55 ns, the mutant form showed constant stability than the wild-type counterpart in respect to the RMSD values throughout the rest of the trajectory (Fig. 8). This result implicates that the mutant Y85N quinone reductase of *E. coli* is more stable than the wild-type form of this enzyme during the interaction with FMN. Eswaramoorthy et al. [31] in their study showed that Tyr85 has an important role in the interaction between two dimmers of the *E. coli* quinone reductase. They have also concluded that changes of amino acid in this position result in the enhancement of chromate reductase activity of the enzyme [31]. In line with this statement, our finding from the RMSD graph also suggested that Y85N mutation in *E. coli* quinone reductase helps in the structural integrity and thus it might increase the activity of this enzyme as well.

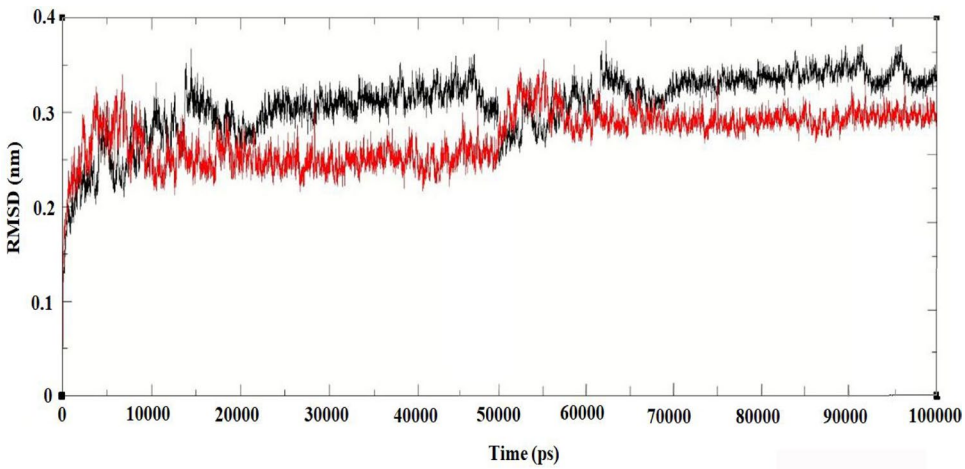

Fig. 8 RMSD of the proteins as functions of time calculated for wild-type quinone reductase from *E. coli* (black) and Y85N mutant (red)

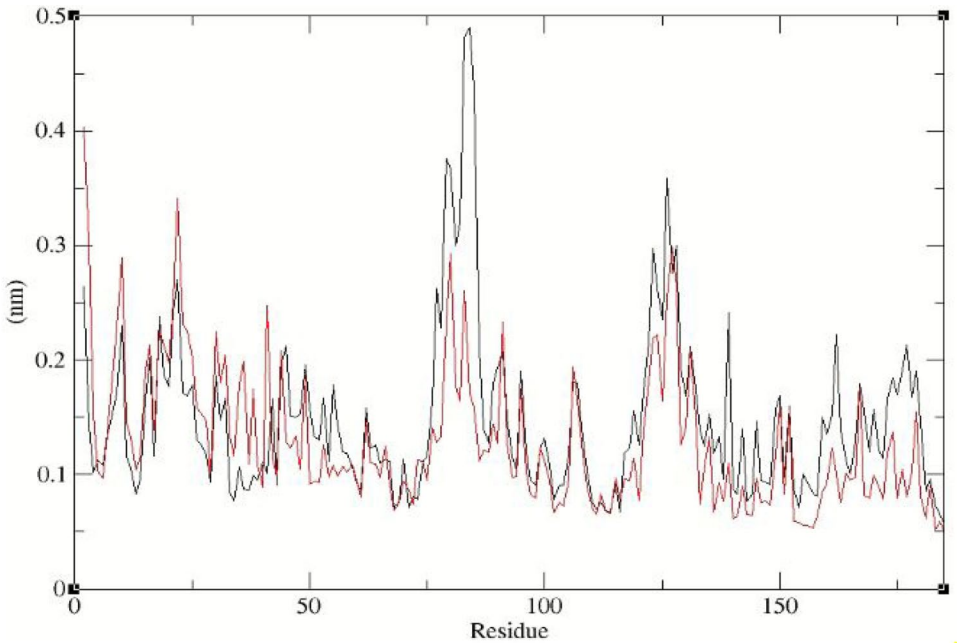

Fig. 9 RMSF of the proteins according to residue numbers calculated for wild-type quinone reductase from *E. coli* (black) and Y85N mutant (red)

4.2 Root mean square fluctuation

Comparative RMSF value clearly shows the structural flexibility of wild-type quinone reductase from *E. coli* than its mutant (Y85N) counterpart. In wild-type quinone reductase of *E. coli*, the RMSF value of Tyr85 residue was recorded as 0.49 nm, while in the mutant enzyme, the Asn85 residue was shown to retain comparatively lesser fluctuation with an RMSF value of 0.26 nm (Fig. 9). This result suggested that the Y85N mutation is a stable mutation which has a significant role in strengthening the protein structure during the interaction with ligand FMN as the Tyr85 is a ligand binding site as well. Within the tetramer of *E. coli* quinone reductase, the dimers interact by a pair of two hydrogen bond networks which also involve the residue Tyr85 [31]. Result from the comparative RMSF graph implied that mutation of Tyr85 to Asparagine residue might have some role in strengthening the bonding network between the dimers of *E. coli* quinone reductase as a less RMSF values has been recorded in case of mutant (Y85N) enzyme. Paul et al. [60], in their study showed greater stability of human NF-κβ enzyme during its binding with a designed small molecule DRG7 according to the RMSF graph likewise the result presented from the RMSD analysis in the present study.

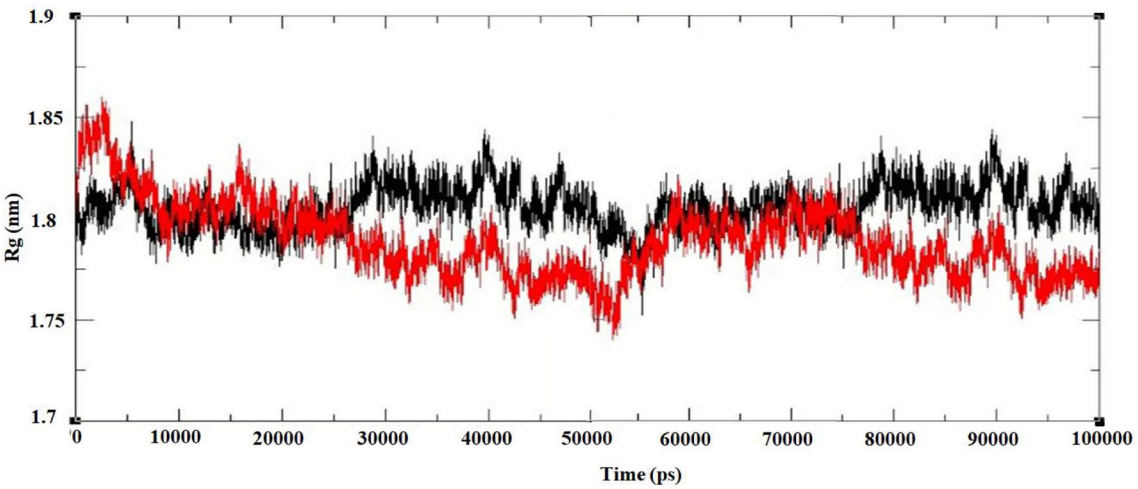

Fig. 10 Rg of the proteins (left) as functions of time calculated for wild-type quinone reductase from *E. coli* (black) and Y85N mutant (red)

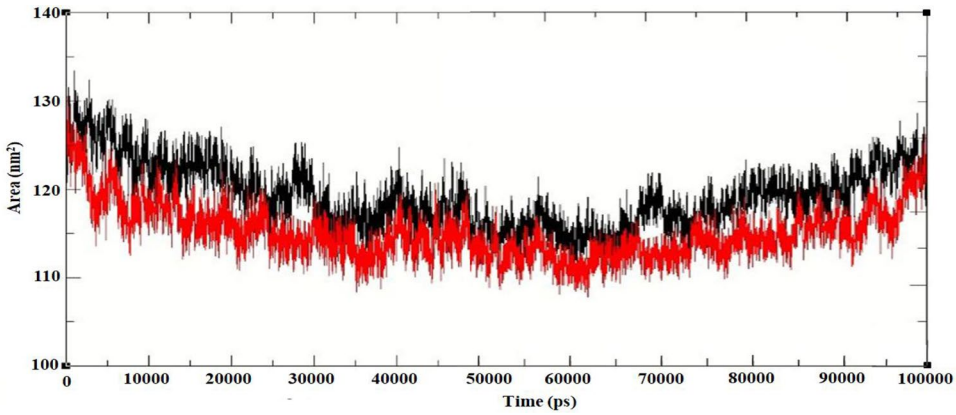

Fig. 11 SASA of the proteins (right) according to residue number for wild-type quinone reductase from *E. coli* (black) and Y85N mutant (red)

4.3 Radius of gyration (Rg)

From the Rg graph, it can be shown that the wild-type *E. coli* quinone reductase has less Rg value compared to mutant one for first 5 ns timescale of MD simulation. Afterward, up to 25 ns both the wild-type and mutant forms of *E. coli* quinone reductase showed the same kind of Rg pattern. After 25 ns timescale of simulation, mutant (Y85N) quinone reductase of *E. coli* represent less Rg value compared to its wild-type form up to the 52 ns timescale. After that, the Rg peak of Y85N mutant gradually raised up to a value of approx 1.8 nm where it meets with the Rg peak of wild-type counterpart of *E. coli* quinone reductase at near about 55 ns of simulation. Within the timescale, 55–76 ns, both the wild-type and mutant forms of the enzyme maintain an overlapped Rg curve after which the Rg values of the mutant *E. coli* quinone reductase gradually started to decline compared to the wild type and finally reached at the value well below 1.8 nm, while the wild-type form ends at an Rg value near about 1.8 nm after the 100 ns of simulation (Fig. 10). This result revealed that the mutant quinone reductase of *E. coli* is more stable than its wild type when interacting with FMN. In the study of Eswaramoorthy et al. [31], it has been reported that the movement of the Tyr85 side chain makes the tetramer of *E. coli* quinone reductase more stable and increase the accessible area of FMN [31]. In consent with the above report, the Rg result of current study implied that in the Y85N mutation, the Asn85 might become more flexible so that it able to make the accessible area of FMN even larger than that of wild-type *E. coli* quinone reductase. Thus, binding of FMN within the cleft of mutant quinone reductase is more stable than its wild-type form.

4.4 Solvent accessible surface area

In this study, the solvent accessible surface area of FMN bound *E. coli* quinone reductase both in its wild-type and mutant forms (Y85N) has been determined up to the 100 ns timescale of MD simulation. It has been shown from the result that the mutant (Y85N) form of *E. coli* quinone reductase has the less solvent accessible area compared to the wild type throughout the whole trajectory of MD simulation (Fig. 11). This result depicted that the mutant quinone reductase of *E. coli* has more compactness in its structure in relation to the wild-type form. Paul et al. [61], in their study, performed a similar type of analysis where they calculated comparative SASA of a bacterial chemotaxis protein CheY from both the mesophilic *E. coli* and thermophilic *Thermotoga maritime* [61]. In this study, SASA determination according to time for both the CheY systems concluded that thermophilic CheY has less SASA value in comparison with mesophilic CheY which implied that thermophilic CheY has greater stability. SASA analysis from the present study is thus in concurs with the hypothesis presented by Paul et al. [61].

4.5 Principal Component Analysis (PCA)

In PCA, the movement of protein backbone has been determined throughout the simulation along two eigenvectors which are called first eigenvector (PC1) and is second eigenvector (PC2). According to the comparative PCA graph of wild-type and mutant (Y85N) quinone reductase from *E. coli*, it can be observed that there has more conformational spaces sampled in the case of FMN bound mutant quinone reductase in related to its wild-type form. These conformational spaces are compact and very close to each other in case of mutant protein while in wild-type form the sampled conformational spaces are scattered from each other and are distantly related (Fig. 12). As sampled conformational space and their distance are significantly related to the flexibility of protein and that a protein will be more stable if it has more conformational space with a less intermediate distance between them, the mutant (Y85N) form of *E. coli* quinone reductase appears as comparatively stable than wild type. Cunha et al. [62], in their study, hypothesized a relation of protein

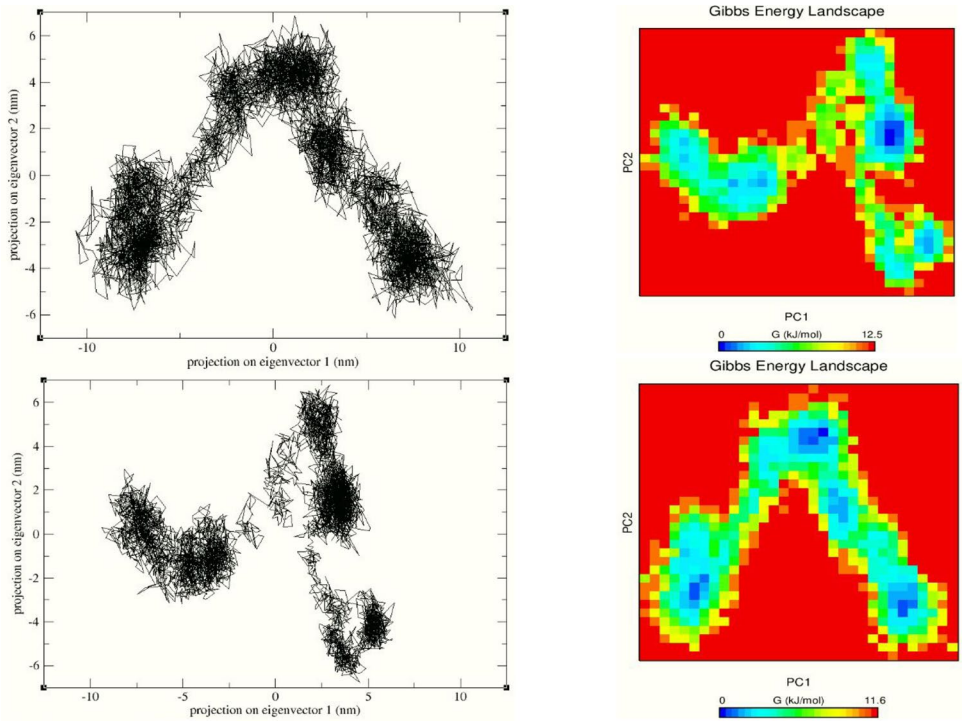

Fig. 12 Principal Component Analysis (PCA) [Left panel] and Gibb's Energy Landscape (GEL) [Right panel] for wild type (upper) and Y85N mutant (lower) quinone reductase from *E. coli*

conformational sampling with its structural stability via de novo design and molecular dynamics simulations. They also stated that the secondary structure of a protein is also coherently associated with the changes of conformational sampling during the protein dynamism [62]. In the current study, it has also been reflected from the PCA that in the case of mutant (Y85N) form of *E. coli* quinone reductase secondary structure integrity is maintained throughout the simulation trajectory compared to its wild-type form as the conformational spaces are linked more adjacent with each other alongside the two eigenvectors (PC1 and PC2).

4.6 Gibb's energy landscape (GEL)

In the present study, GEL was analyzed for the wild-type and mutant (Y85N) quinone reductase from *E. coli* bound with the ligand FMN. 2D Gibbs free energy plots have been generated by using the two eigenvectors (PC1 and PC2), obtained from the principal component analysis. From the comparative GEL plots of the wild-type and mutant forms of *E. coli* quinone reductase, it can be showed that the mutant form of the enzyme has more number conformational spaces with low energy state (blue patches), while the wild-type form of the enzyme has less number of conformational space highlighted with blue patches which depict that the wild-type protein is comparatively less stable during the interaction with FMN. The energy hotspot bar also resulted from that wild-type quinone reductase has a higher maxima of -12.5 kJ/mol in comparison with the mutant form of the enzyme which has an energy maxima of -11.6 kJ/mol. These energy values also represent that mutant (Y85N) quinone reductase has more integrity in its structure compared to the wild type (Fig. 12). The structural integrity of protein–ligand complex is notably related to free energy terms, and it has been well established. Bharatiy et al. [63], in their study, have designed an industrially sustainable α-carbonic anhydrase (α-CA) and studied its dynamics behavior using MD simulation [63]. In this study, they have analyzed the free energy landscape from the MD simulation trajectories of the simulated systems of the wild-type mesophilic, thermophilic, and mutant α-CA to present the highest stability of mutant counterpart. In their study, they have shown the stability of the mutant enzyme in light of Gibb's energy plots which is well relevant with the result of stability-energy co-relationship as depicted from the present study.

5 Conclusion

There are several classes of bacterial chromate reductase like enzyme, namely quinone reductases, FMN-reductase, nitroreductases, and NADPH-dependent, which help in the chromate bioremediation. Sequence conservativeness study has identified important residues in these classes of enzyme which play important role in substrate specificity. Domain and motif analyses also suggested that these enzymes share a significant similarity in their secondary

structure components. Investigation of FMN binding with these classes of enzyme depicted that FMN plays a crucial role in enzymatic catalysis. In reference to the previous literature, in vitro mutational studies of FMN binding and its specificity in regulating the enzymatic reaction have been validated through molecular docking. MD simulation study revealed that the Y85N of *E. coli* quinone reductase is more stable compared to the wild-type form of the enzyme during the interaction with ligand FMN. The present study based on these structural and dynamics aspects would help to draw ideas about the tailor-made design of enzyme which can efficiently reduce environmental chromate pollution.

Acknowledgments Authors are grateful to the Bioinformatics Facility, Department of Biotechnology, North Orissa University, Baripada, India, for the provision of computational support. The work was partially conducted in the context of the Bioinformatics Resources and Applications Facility (BRAF), C-DAC, Pune, India.

Compliance with ethical standards

Conflict of interest The authors declare that they have no conflict of interest.

References

1. Fei Y, Liu C (2016) Detoxification and resource recovery of chromium-containing wastes. In: Prasad MNV, Shih K (eds) Environmental materials and waste. Academic Press, Cambridge, pp 265–284
2. Islam S, Islam F, Bakar MA, Das S, Bhuiyan HR (2013) Heavy metals concentration at different tannery wastewater canal of Chittagong city in Bangladesh. Int J Agri Environ Biotechnol 6:355–362
3. Sivaram NM, Barik D (2019) Toxic waste from leather industries. In: Debabrata B (ed) Energy from Toxic Organic Waste for Heat and Power Generation. Woodhead Publishing, Cambridge, pp 55–67
4. CERCLA Priority List of Hazardous Substances (2017). Agency for Toxic Substances and Disease Registry, USA. Available online: https://www.atsdr.cdc.gov/spl/. (accessed on 11 Feb 2020)
5. Kundu D, Dey S, Sen Raychaudhuri S (2018) Chromium (VI) – induced stress response in the plant plantago ovata forsk in vitro. Gene Environ 40:21
6. Bhattacharya A, Gupta A, Kaur A, Malik D (2019) Alleviation of hexavalent chromium by using microorganisms: insight into the strategies and complications. Water Sci Technol 79:411–424
7. Thatoi H, Das S, Mishra J, Rath BP, Das N (2014) Bacterial chromate reductase, a potential enzyme for bioremediation of hexavalent chromium: a review. J Environ Manage 146:383–399
8. Kamaludeen SPB, Megharaj M, Juhasz AL, Sethunathan N, Naidu R (2003) Chromium-microorganism interactions in soils: remediation implications. Rev Environ Contam Toxicol 178:93–164
9. Barrera-Díaza CE, Lugo-Lugoa V, Bilyeu B (2012) A review of chemical, electrochemical and biological methods for aqueous Cr(VI) reduction. J Hazard Mater 223–224:1–12
10. Dhal B, Thatoi H, Das NN, Pandey BD (2013) Chemical and microbial remediation of hexavalent chromium from contaminated soil and mining/metallurgical solid waste: a review. J Hazard Mater 250:272–291
11. Narayani M, Shetty KV (2013) Chromium-resistant bacteria and their environmental condition for hexavalent chromium removal: a review. Crit Rev Environ Sci Technol 43:955–1009
12. Ohtake H, Cervantes C, Silver S (1987) Decreased chromate uptake in *Pseudomonas fluorescens* carrying a chromate resistance plasmid. J Bacteriol 169:3853-e3856
13. James BR (1996) The challenge of remediating chromium-contaminated soils. Environ Sci Technol 30:248A-251A
14. Bhateria R, Dhaka R (2017) Biological strategies for detoxification of hexavalent chromium. Int J Pharma Bio Sci 8:35–48
15. Park CH, Keyhan M, Wielinga B, Fendorf S, Matin A (2000) Purification to homogeneity and characterization of a novel *Pseudomonas putida* chromate reductase. Appl Environ Microbiol 66:1788–1795
16. James BR (2001) Remediation-by-reduction strategies for chromate-contaminated soils. Environ Geochem Health 23:175–179
17. Ackerley DF, Gonzalez CF, Keyhan M, Blake R, Matin A (2004) Mechanism of chromate reduction by the *Escherichia coli* protein, NfsA, and the role of different chromate reductases in minimizing oxidative stress during chromate reduction. Environ Microbiol 6:851–860
18. Jin H, Zhang Y, Buchko GW, Varnum SM, Robinson H, Squier TC, Long PE (2012) Structure determination and functional analysis of a chromate reductase from *Gluconacetobacter hansenii*. PLoS ONE 7:e42432
19. Das S, Mishra J, Das SK, Pandey S, Rao DS, Chakraborty A, Sudarshan M, Das N, Thatoi H (2014) Investigation on mechanism of Cr (VI) reduction and removal by *Bacillus amyloliquefaciens*, a novel chromate tolerant bacterium isolated from chromite mine soil. Chemosphere 96:112–121
20. Krishnaraj RN, Samanta D, Kumar A, Sani R (2017) Bioprospecting of thermostable cellulolytic enzymes through modeling and virtual screening method. Can J Biotechnol 1:19–25
21. Sharma NK, Jha Priyanka KK (2010) Molecular docking; an overview. J Adv Sci Res 1:67–72
22. Huang SY, Zou X (2010) Advances and challenges in protein ligand docking. Int J Mol Sci 11:3016–3034
23. Corpet F (1988) Multiple sequence alignment with hierarchical clustering. Nucleic Acids Res 16:10881–10890
24. Ackerley DF, Barak Y, Lynch SV, Curtin J, Matin A (2006) Effect of chromate stress on *Escherichia coli* K-12. J Bacteriol 188:3371–3381
25. Altschul SF, Gish W, Miller W, Myers EW, Lipman DJ (1990) Basic local alignment search tool. J Mol Biol 215:403–410
26. Lawrence AK, Mezulis S, Yates CM, Wass MN, Sternberg MJE (2015) The Phyre2 web portal for protein modeling, prediction and analysis. Nat Protoc 10:845–858
27. Lindahl E, Azuara C, Koehl P, Delarue M (2006) NOMAD-Ref: visualization, deformation and refinement of macromolecular structures based on all-atom normal mode analysis. Nucleic Acids Res 34:W52–W56
28. Laskowski RA, Jabłońska J, Pravda L, Svobodová Vařeková R, Thornton JM (2018) PDBsum: structural summaries of PDB entries. Protein Sci 27:129–134
29. Colovos C, Yeates TO (1993) Verification of protein structures: patterns of nonbonded atomic interactions. Protein Sci 2:1511–1519
30. Luthy R, Bowie JU, Eisenberg D (1992) Assessment of protein models with three-dimensional profiles. Nature 356:83–85
31. Eswaramoorthy S, Poulain S, Hienerwadel R, Bremond N, Sylvester MD, Zhang YB, Berthomieu C, Lelie DVD, Matin A (2012) Crystal structure of ChrR—A quinone reductase with the capacity to reduce chromate. PLoS ONE 7:e36017

32. Trott O, Olson AJ (2010) AutoDock vina: improving the speed and accuracy of docking with a new scoring function, efficient optimization, and multithreading. J Comput Chem 31:455–461
33. Emsley P, Cowtan K (2004) Coot: model-building tools for molecular graphic. Acta Cryst D Biol Crystallogr 60:2126–2132
34. Schomburg I, Chang A, Schomburga D (2002) BRENDA, enzyme data and metabolic information. Nucleic Acids Res 30:47–49
35. DeLano WL (2002) The PyMOL molecular graphics system; San Carlos, CA: DeLano Scientific. https://www.pymol.org
36. Pettersen EF, Goddard TD, Huang CC, Couch GS, Greenblatt DM, Meng EC, Ferrin TE (2004) UCSF chimera–a visualization system for exploratory research and analysis. J Comput Chem 25:1605–1612
37. Antunes DA, Moll M, Devaurs D, Jackson KR, Lizée G, Kavraki LE (2017) DINC 2.0: a new protein-peptide docking webserver using an incremental approach. Cancer Res 77:e55–e57
38. Quevillon E, Silventoinen V, Pillai S, Harte N, Mulder N, Apweiler R, Lopez R (2005) InterProScan: protein domains identifier. Nucleic Acids Res 33:W116–W120
39. Kumar S, Stecher G, Tamura K (2016) MEGA7: molecular evolutionary genetics analysis version 7.0 for bigger datasets. Mol Biol Evol 33:1870–1874
40. Pall S, Abraham MJ, Kutzner C, Hess B, Lindahl E (2015) Tackling exascale software challenges in molecular dynamics simulations with GROMACS. In: Markidis S, Laure E (eds) Solving software challenges for exascale, vol 8759. Springer International Publishing, Switzerland, London, pp 3–27
41. van Gunsteren WF, Billeter SR, Eising AA, Hünenberger PH, Krüger P, Mark AE, Scott WRP, Tironi IG (1996) Biomolecular Simulation: The GROMOS96 Manual and User Guide vdf Hochschulverlag AG an der ETH Zürich and BIOMOS b.v.: Zürich, Groningen
42. Miyamoto S, Kollman PA (1992) SETTLE: an analytical version of the SHAKE and RATTLE algorithm for rigid water models. J Comput Chem 13:952–962
43. Weber W, Hünenberger PH, McCammon JA (2000) Molecular dynamics simulations of a polyalanine octapeptide under ewald boundary conditions: influence of artificial periodicity on peptide conformation. J Phy Chem B 104:3668–3675
44. Hess B, Bekker H, Berendsen H, Fraaije J (1997) LINCS: a linear constraint solver for molecular simulations. J Comput Chem 18:1463–1472
45. Darden T, Perera L, Li L, Pedersen L (1999) New tricks for modelers from the crystallography toolkit: the particle mesh ewald algorithm and its use in nucleic acid simulations. Structure 7:R55–R60
46. Vaught A (1996) Graphing with gnuplot and xmgr, Linux Journal. https://dl.acm.org/citation.cfm?id=326334
47. Amadei A, Linssen AB, Berendsen HJ (1993) Essential dynamics of proteins. Proteins 17:412–425
48. Amadei A, Ceruso MA, Nola AD (1999) On the convergence of the conformational coordinates basis set obtained by the essential dynamics analysis of proteins' molecular dynamics simulations. Proteins 36:419–424
49. Deng P, Tan X, Wu Y, Bai Q, Jia Y, Xiao H (2015) Cloning and sequence analysis demonstrate the chromate reduction ability of a novel chromate reductase gene from *Serratia* sp. Exp Ther Med 9:795–800
50. Opperman DJ, van Heerden E (2008) A membrane-associated protein with Cr(VI)-reducing activity from *Thermus scotoductus* SA-01. FEMS Microbiol Lett 280:210–218
51. Gorman J, Shapiro L (2005) Crystal structures of the tryptophan repressor binding protein WrbA and complexes with flavin mononucleotide. Protein Sci 14:3004–3012
52. Opperman DJ, Sewell BT, Litthauer D, Isupov MN, Littlechild JA, van Heerden E (2010) Crystal structure of a thermostable old yellow enzyme from *Thermus scotoductus* SA-01. Biochem Biophys Res Commun 393:426–431
53. Wang ZX, Li L, Dong YH, Su XD (2014) Structural and biochemical characterization of MdaB from cariogenic *Streptococcus mutans* reveals an NADPH-specific quinone oxidoreductase. Acta Crystallogr D Biol Crystallogr 70:912–921
54. Herrou J, Czyz DM, Willett JW, Kim HS, Chhor G, Babnigg G, Kim Y, Crosson S (2016) WrpA Is an atypical flavodoxin family protein under regulatory control of the *Brucella abortus* general stress response system. J Bacteriol 198:1281–1293
55. Ball J, Salvi F, Gadda G (2016) Functional annotation of a presumed nitronate monoxygenase reveals a new class of NADH: quinone reductases. J Biol Chem 291:21160–21170
56. Pradhan SK, Singh NR, Rath BP, Thatoi HN (2016) Bacterial chromate reduction: a review of important genomic, proteomic and bioinformatic analysis. Crit Rev Env Sci Tec 46:21–22
57. Borshchevskiy V, Round E, Bertsova Y, Polovinkin V, Gushchin I, Ishchenko A, Kovalev K, Mishin A, Kachalova G, Popov A, Bogachev A, Gordeliy V (2015) Structural and functional investigation of flavin binding center of the NqrC subunit of sodium-translocating NADH: quinone oxidoreductase from *Vibrio harveyi*. PLoS ONE 10:e0118548
58. Li X, Chow DC, Tu SC (2006) Thermodynamic analysis of the binding of oxidized and reduced FMN cofactor to *Vibrio harveyi* NADPH-FMN oxidoreductase FRP apoenzyme. Biochemistry 45:14781–14787
59. Muralidhara BK, Chen M, Ma J, Wittung-Stafshede P (2005) Effect of inorganic phosphate on FMN binding and loop flexibility in *Desulfovibrio desulfuricans* apo-flavodoxin. J Mol Biol 349:87–97
60. Paul M, Panda MK, Thatoi H (2019) Developing Hispolon-based novel anticancer therapeutics against human (NF-κβ) using in-silico approach of modelling, docking and protein dynamics. J Biomol Struc Dyn 37:3947–3967
61. Paul M, Hazra M, Barman A, Hazra S (2014) Comparative molecular dynamics simulation studies for determining factors contributing to the thermostability of chemotaxis protein CheY. J Biomol Struc Dyn 32:928–949
62. Cunha KC, Rusu VH, Viana IF, Marques ET, Dhalia R, Lins RD (2015) Assessing protein conformational sampling and structural stability via de novo design and molecular dynamics simulations. Biopolymers 103:351–361
63. Bharatiy S, Hazra M, Paul M, Mohapatra S, Samantaray D, Dubey RC, Sanyal S, Datta S, Hazra S (2016) In silico designing of an industrially sustainable carbonic anhydrase using molecular dynamics simulation. ACS Omega 1:1081–1103